Int. J. Electrochem. Sci., 17 **(2022)** Article Number: 220751, doi: 10.20964/2022.07.55

International Journal of
ELECTROCHEMICAL
SCIENCE
www.electrochemsci.org

Corrosion Behavior of Titanium and Titanium Alloys in Ringer´s Solution

F. Almeraya-Calderón[1], Jesús M. Jáquez-Muñoz[1,2,], M. Lara-Banda [1], P. Zambrano-Robledo[1], J. A. Cabral-Miramontes[1]., Alejandro Lira-Martínez[2], F. Estupinán-López[1]., C. Gaona Tiburcio[1]*

[1] Universidad Autónoma de Nuevo León, Facultad de Ingeniería Mecánica y Eléctrica, Centro de Investigación e Innovación en Ingeniería Aeronáutica (CIIIA), Av. Universidad s/n, Ciudad Universitaria, San Nicolás de los Garza, Nuevo León 66455, México
[2] Universidad Autónoma de Ciudad Juárez, Instituto de Ingeniería y Tecnología (IIT), Av. Del Charro 450 Nte Ciudad Juárez Chihuahua 32584. México.
[*]E-mail: jesus.jaquezmn@uanl.edu.mx

Received: 13 March 2022 / *Accepted:* 29 April 2022 / *Published:* 6 June 2022

Titanium and its alloys are employed as medical materials because of their low Young's modulus, excellent biocompatibility, and superior corrosion resistance. This work aimed to characterize the electrochemical behavior of titanium Ti-CP2 and alloys Ti-6Al-2Sn-4Zr-2Mo, and Ti-6Al-4V. Ti and Ti-alloys were exposed to Ringer´s solution at room temperature. The electrochemical characterization was made by cyclic potentiodynamic polarization (CPP) and electrochemical noise technique (EN). Two different methods filtered EN signal, the polynomial method and the potential spectral density (PSD). Also, the Wavelets method, where energy dispersion plots were obtained. Results indicated that Ti-6Al-2Sn-4Zr-2Mo presented less dissolution when exposed in Ringer analysis by ψ0. The wavelet method showed a diffusion process occurring on the surface.

Keywords: Titanium Alloys, Biomedical, Electrochemical Corrosion, Electrochemical Noise, FFT, Wavelets.

1. INTRODUCTION

Due to mechanical and good corrosion properties, titanium alloys have been used in marine, aeronautic, aerospace, chemical, and biomedical industries [1]. Different types of Ti-alloys have been employed for implant applications. Titanium has four classifications: α, near-α, α+β, and β metastable. Titanium α is commercially pure (Ti CP); this type of alloy presents a good corrosion resistance, but mechanical resistance is low compared with other Ti-alloys [2,3]. To increase the mechanical resistance and improve corrosion resistance elements such as Mo, V, Nb, or Cr (β stabilizers). The addition of Mo in Ti alloys improves the corrosion resistance of alloys[4]. Also, Zr (neutral element) was studied in Ti-

alloys, and results showed that zirconium reduces material dissolution compared with Ti CP. In addition, Zr creates a more homogenous oxide film, increasing the corrosion resistance [5]. For that reason, the near-α alloy such as Ti-6Al-2Sn-4Zr-2Mo has been used with combined mechanical and corrosion resistance [6].

However, the research employs alloys with greater quantities of β stabilizers looking for increased mechanical resistances creating α+β alloys, with percentages from 4 to 8% of β stabilizers [7]. The most employed Ti-alloy is Ti-6Al-4V in all industries; Ti-6Al-4V is the alternative to Ti CP because of its better mechanical properties [8]. However, vanadium and aluminum are toxic elements for body interaction, and the dissolution of V and Al ions can provoke Alzheimer's, genotoxicity, and peripheral neuropathy [9].

The biocompatibility is a crucial factor in employing alloys with elements such as Zr, Ta, Mo, or Sn as an option of Ti -6Al-4V. Research focuses on finding alloys that can be employed for orthopedic and dental implants [10]. Zirconium pertains to the same titanium group; for that reason, both present good biocompatibility and corrosion resistance and make them candidates for different types of prosthesis [11].

However, corrosion problems can affect titanium, mainly when the electrolyte contains Cl^- ions [12,13]. Authors have reported different types of corrosion, such as Sikora et al., where pitting corrosion attacks due to crevices and corrosion [14]. Also, the material can lose mass in cathodic potentials [15].

Corrosion resistance increase with the addition of alloying elements. The corrosion kinetics decrease with Ti-6Al-4V ELI compared to pure titanium in phosphate-buffered solution (PBS), indicating that alloy has better corrosion resistance [16]. Also, a diffusion process has been reported by various authors when different salts are in media [17]. However, some ions, such as Cl^-, Ca^-, Mg^- and K^- passive layers became unstable, and the growth was non-homogenous [18,19].

Diverse techniques can be used to study the electrochemical behavior of materials. Cyclic potentiodynamic polarization (CPP) apports information about the reaction in the cathodic and anodic processes [20]. Also, it gives information on the type of corrosion, corrosion rates, and stability of the passive layer [21]. The other technique used is electrochemical noise (EN). EN is employed to monitor corrosion and has different methods to analyze. Besides, it is a non-perturbative technique and is helpful to detect localized corrosion processes [22,23].

The comparison of Ti CP2 and Ti-6Al-4V with Ti-6Al-2Sn-4Zr-2Mo is essential for implant surface technology options for non-toxic implants. The study of the electrochemical behavior of those alloys will provide apport information to choose better alloys. The aim of this work is to study the electrochemical behavior of Ti CP2, Ti-6Al-2Sn-4Zr-2Mo, and Ti-6Al-4V immersed in Ringer´s solution as a body simulator at room temperature. The electrochemical techniques used were cyclic potentiodynamic polarization and electrochemical noise. Microstructural characterization was conducted using scanning electron microscopy (SEM) and energy-dispersive X-ray spectroscopy (EDS).

2. MATERIALS AND METHODS

2.1. Materials

The materials used in this work were Ti CP2 and alloys: Ti-6Al-2Sn-4Zr-2Mo, and Ti-6Al-4V, used under as-received conditions. The chemical composition of Ti-alloys was obtained by X-ray fluorescence is shown in Table 1.

Table 1. Chemical composition of titanium and its alloys (wt %).

Elements	Ti CP2	Alloys	
		Ti-6Al-2Sn-4Zr-2Mo	Ti-6Al-4V
Fe	0.038 ± 0.005	–	0.21 ± 0.01
Al	–	6.75 ± 0.20	7.14 ± 0.37
V	–	–	4.03 ± 0.08
Zr	–	4.18 ± 0.01	–
Cr	–	–	–
Mo	–	1.99 ± 0.008	–
Sn	–	2.08 ± 0.01	–
Ti	99.94 ± 0.005	84.65 ± 0.19	87.71 ± 0.36

2.2. Microstructural Characterization

Specimens were prepared according to ASTM E3-11 (2017) [24]. Polishing was done employing SiC grit paper until 4000 grades. Also, cleaning for 10 minutes using ultrasonic in ethanol and deionized water was performed. Etching of polish samples was with Kroll solution composed of HF 3 mL, HNO3 5 mL, and water 100 mL according to ASTM E 407[25].

The microstructural analysis was investigated using scanning electron microscopy (SEM) for identifying the micrographs by SEM were taken using a backscattered electron (BSE) detector. 500 × and 1000 × operating at 20 kV, WD = 14 mm. The chemical composition of these alloys was obtained by energy-dispersive X-ray spectroscopy (EDS).

2.3. Electrochemical Test

2.3.1. Cyclic Potentiodynamic Polarization

In the Cyclic Potentiodynamic Polarization (CPP), the following parameters were used: the potential scan range was applied between -1.0 and 1.0 V (complete polarization cycle) from the open circuit potential (OCP) and sweep rate of 0.06 V/min, according to ASTM G5-13 [26] and ASTM G61-86 standards [27]. Corrosion experiments were performed by immersion in Ringer's solution (NaCl 9 g, KCl 0.425 g, $CaCl_2$ 0.119 g, $NaHCO_3$ 01 g in 1 l of aqueous solution). The titanium and its alloys specimens had a surface area of 1.0 cm^2, The corrosion cell consisted of a working electrode (Ti and Ti-

alloys), a saturated calomel electrode [SCE, (0.244V versus SHE at 25 °C)] as reference electrode, and a platinum mesh served as counter electrode for the current measurements.

In CPP curves, analysis of the anodic and cathodic reactions and the hysteresis curve can yield information about the mechanism of corrosion in the system and the corrosion rates. The Tafel extrapolation of potentiodynamic polarization curves is employed to determine the corrosion current density, i_{corr} ($mA \cdot cm^{-2}$), and corrosion rate [28,29].

The corrosion kinetic behavior can be observed using potentiodynamic polarization through cathodic and anodic reactions in polarization curves. The corrosion rate in terms of penetration (mm/s) is one of the main parameters obtained by potentiodynamic polarization curves, according to Faraday's law (Equation (1)) [30-32].

$$C.R = \frac{k \cdot i_{corr}}{\rho \cdot E \cdot W} \qquad (1)$$

Where E.W = equivalent weight, ρ = density in g/cm^3, k= a constant, and i_{corr} = current density in $\mu A/cm^2$.

2.3.2. Electrochemical Noise

The Electrochemical Noise (EN) technique was conducted by ASTM G199-09 standard [33]. The corrosion cell consisted of two nominally identical working electrodes (WE1 and WE2) and, as reference electrodes (RE), a saturated calomel electrode (SCE). Each experiment's data number was 4096 at a scanning rate of 1 data/s. The trend remotion (with polynomial 9°) and Fast Fourier Transform (FFT) were realized in a MATLAB 2018a software [34-35]. The equipment used was a Gill-AC potentiostat/galvanostat/ZRA (Zero Resistance Ammeter) from ACM Instruments. The test was made in triplicate at room temperature.

2.3.3. Polynomial Method

It is necessary to filter the signal to eliminate DC because it creates false frequencies and interferes in PSD analysis. The polynomial method is calculated by equation 2, where x_n is the EN signal with all the components, p_o is the polynomial at n-th term (a_i), "n" is the time, and y_n is the signal without trend [36].

$$y_n = x_n - \sum_{i=0}^{p_o} a_i n^i \qquad (2)$$

2.3.4. Power Spectral Density

Spectral density is calculated using PSD analysis equations to transform a signal in time-domain to frequency-domain employing an FFT (with a polynomial filter applied).

$$R_{xx}(m) = \frac{1}{N}\sum_{n=0}^{N-m-1} x(n) \cdot x(n+m), \text{ values from } 0 < m < N \quad (3)$$

$$\Psi_x(k) = \frac{\gamma \cdot t_m}{N} \cdot \sum_{n=1}^{N} (x_n - \bar{x}_n) \cdot e^{\frac{-2\pi k n^2}{N}} \quad (4)$$

The PSD interpretation is based on the specter's slope. The slope could help determine the corrosion type. It is named β_x and is represented in the following equation.

$$log\Psi_x = -\beta_x \, log \, f \quad (5)$$

The ψ^0 (frequency zero limits) permits interpreted materials dissolution due to PSD's power associated with the system's total energy [37]. The material dissolution is only can be interpreted with the current PSD. Table 2 was proposed by Mansfeld, and this table was adapted to decibels [38-39].

Table 2. Intervals of β to determine the corrosion type [39].

Corrosion type	dB(V)·decade^{-1}		dB(A)·decade^{-1}	
	Minimum	**Maximum**	**Minimum**	**Maximum**
Uniform	0	–7	0	–7
Pitting	–20	–25	–7	–14
Passive	–15	–25	–1	1

2.3.5. Wavelets Method

The wavelets method decomposes a signal by a high-low filter application and calculates the energy of each detail crystal (high frequency).

$$E = \sum_{n-1}^{N} x_n^2 \quad (6)$$

Moreover, energy fractions of details and approximation are calculated by equations 13:

$$ED_j^d = \frac{1}{E}\sum_{n=1}^{N} d_{j,n}^2 \quad ED_j^s = \frac{1}{E}\sum_{n=1}^{N} s_{j,n}^2 \quad (7)$$

The total of energy analyzed is equal to each component energy of the wavelet transform, equation 14:

$$E = ED_j^s \sum_{j=1}^{j} ED_j^d \qquad (8)$$

The number of crystals to analyze in this research is 8 details. The energy accumulated in the first crystals (D1 to D3) is related to the metastable process. The energy accumulated in intermediate crystals (D4 to D6) is related to localized processes. Finally, the energy accumulated in the last crystals (D7 and D8) is associated with the long-time process as diffusion, controlled, or generalized processes [40]. The following equation is to determine the time range of each crystal.

$$\left(c_1^j, c_2^j\right) = \left(2^{-j}\Delta t, 2^{j-1}\Delta t\right) \qquad (9)$$

Where c is the crystal, and Δt is the time display. Table 3 shows each crystal scale range of scale of each crystal in seconds and Hz. High-frequency crystals Crystal of high frequency are the first, and low-frequency phenomena are presented on the last crystals.

Table 3. Ranges of crystals scale

Crystal (D)	Scale (s)	Scale (Hz)
1	1 - 2	1 - 0.5
2	2 - 4	0.5 - 0.25
3	4 - 8	0.25 - 0.125
4	8 -16	0.125 - 0.0625
5	16 - 32	0.0625 - 0.3125
6	32 - 64	0.03125 - 0.015625
7	64 - 128	0.015625 - 0.00781
8	128 - 256	0.00781 - 0.00390

3. RESULTS AND DISCUSSION

3.1. SEM microstructural analysis

The microstructures of the samples in initial conditions were analyzed by SEM. Figure 1a shows SEM surface micrograph using a backscattered electron (BES) detector for Ti CP2, where an matrix of

α phase microstructure for Ti CP2, with large grain size. Figure 1b shows α-phase grains with unions in the β phase of the Ti-6Al-2Sn-4Zr-2Mo microstructure. Figure 1c shows the Ti-6Al-4V microstructure; this one is fine and equiaxial. The vanadium presence in Ti-6Al-4V increases the distribution of the β phase and is presented in a spherical way.

The SEM analysis indicates that the porosity of the samples under study was diameters of 1 to 2 µm. Microstructural analysis revealed porosity for samples. It is auspicious corrosion because pores are energy concentrators [41]. Nevertheless, although porosity can provoke localized corrosion, the material can repassivate again for the breakdown and regeneration of the layer [42].

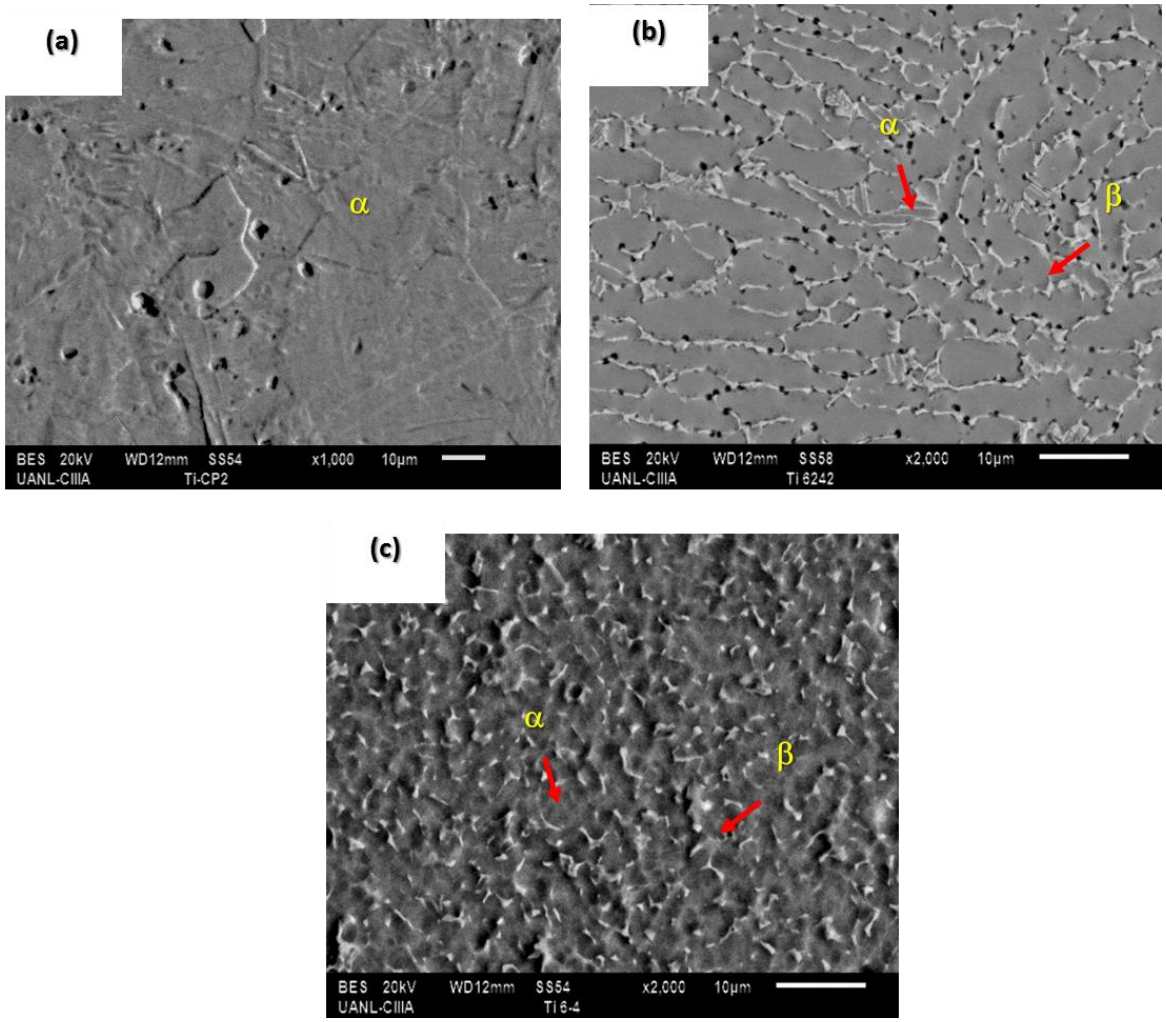

Figure 1. SEM-BES micrograph of titanium and its alloys (initial conditions): (a) Ti CP2. (b) Ti-6Al-2Sn-4Zr-2Mo, (c) Ti-6Al-4V

3.2. Electrochemical measurements

3.2.1. Cyclic Potentiodynamic Polarization

Figure 2 shows the CPP of Titanium and its alloys immersed in Ringer solution. Ti-6Al-2Sn-4Zr-2Mo presented the lower E_{corr} (442 mV) and higher i_{corr} (8.36×10^{-5} mA/cm^2). Those results can be

related to a higher corrosion rate in figure 3 (7.27×10^{-4} mm/year). Also, lower E_{corr} indicates that anodic reactions occur at lower potentials. However, the passivation range is 1222 mV, the higher of all samples, meaning that the passive layer created is stable and effective. Besides, the i_{corr} value of the back curve is lowest for Ti-6Al-2Sn-4Zr-2Mo (1.91×10^{-5}) than for Ti CP2, which results in a more effective passive layer have a lower dissolution. The passive layer of Ti-alloys with vanadium elements showed a rapid dissolution [43]. In this research, the behavior of the passive layer in the reverse CPP showed how Ti-6l-4V has a higher i_{corr} (1.31×10^{-4} A/cm^2) than Ti-6Al-2Sn-4Zr-2Mo (3.94×10^{-5}). The reverse curve gives information about passive layer behavior. In this case, a passive layer of Ti-6Al-4V presents a higher corrosion kinetic. Contrarily, the Ti-6Al-2Sn-4Zr-2Mo passive layer showed a higher corrosion resistance in CPP.

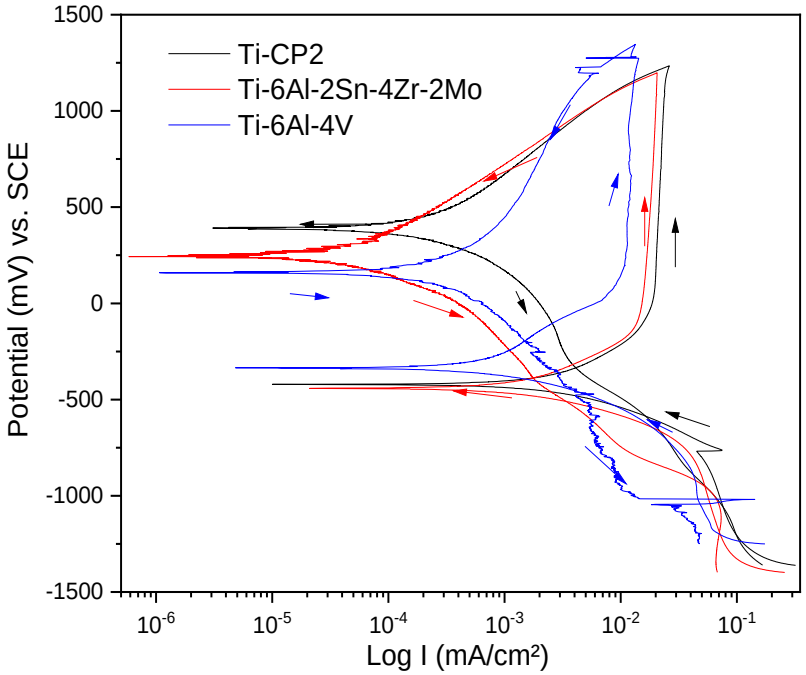

Figure 2. Cyclic Potentiodynamic Polarization curves of titanium and its alloys exposed on Ringer´s solution.

In contrast, Ti-6Al-4V presented the highest E_{corr} (–335 mV) and the lower i_{corr} (4.48×10^{-5} mA/cm^2), and they are related to the corrosion rate in figure 3, where Ti-6Al-4V obtained 4.17×10^{-4} mm/year, being the lowest value. However, the passivation range (see table 4) is lower (1053 mV), indicating more activation. This can be prejudicial for the human body because metals ions of vanadium are not compatible. A better tendency to passivation and lowered current densities when titanium is alloyed with Zr than Ti-6Al-4V has been reported [43-45]. Also, a trend to more positive potentials indicates the need for more energy to initialize the corrosion process, as is shown in CPP. However, an E_{corr} high does not mean a lower corrosion kinetic.

All the samples presented negative hysteresis, meaning that a uniform corrosion process was present in all samples. The return curve shows the behavior of the passive layer created on the surface. All the passive layers presented the dissolution process after hysteresis. However, Ti CP2 presented a higher current density value (1.55×10^{-4} mA/cm^2) in the back curve, meaning that dissolution of the passive layer is higher. In contrast, Ti-6Al-2Sn-4Zr-2Mo presented presented a value of 3.94×10^{-5} mA/cm^2), meaning that the passive layer will be more stable, and the dissolution process will be slower than in the other two titanium.

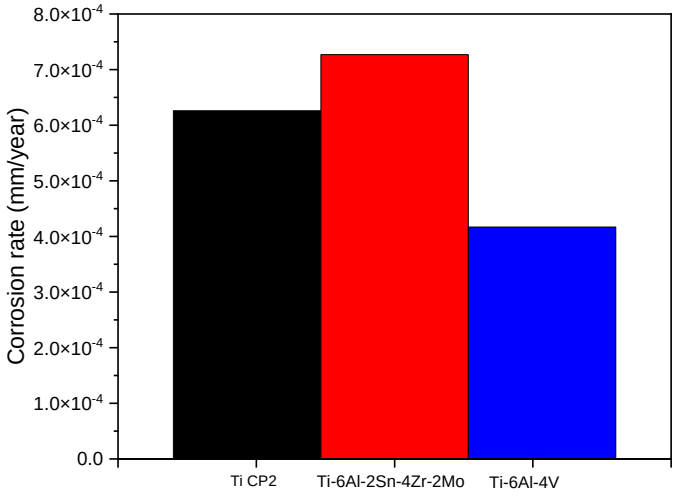

Figure 3. Corrosion rates of titanium and its alloys exposed on Ringer´s solution.

Vasilescu et al [44], have reported the generation of a passive layer with chloride, potassium, and calcium when alloys are exposed to Ringer´s solution. Also, they reported the generation of different oxides when alloys have different elements. Authors have determined that ZrO_2 has better stability and protection quality than TiO_2, and oxides generated by vanadium can destroy the passivity of titanium [45].

Table 4. Parameters obtained by CPP for Titanium and its alloys exposed on Ringer´s solution.

Alloys	**E_{corr} (V)**	**i_{corr} (mA/cm^2)**	**i_{corr} back (mA/cm^2)**	**Histeresys**	**Range passive (V)**
Ti CP2	–421	7.16×10^{-3}	1.05×10^{-4}	Negative	1154
Ti-6Al-2Sn-4Zr-2Mo	–442	8.36×10^{-3}	1.91×10^{-5}	Negative	1222
Ti-6Al-4V	–335	4.48×10^{-3}	3.31×10^{-5}	Negative	1053

3.2.2. Electrochemical Noise

The EN technique can give information related to processes occurring in material surface, pitting, diffusion, passivation, etc. The stability is due to EN not being perturbed by an external source, and the behavior presented is for the reaction of metal in the electrolyte.

3.2.3. Power Spectral Density

Figure 4 shows the behavior of ECN PSD of Titanium and its alloys. The Ti CP2 presents the higher value of ψ^0, being 107.36 dBi $(A^2 \cdot Hz^{-1})^{1/2}$, meaning a faster material dissolution, but in this case, the dissolution is of a passive layer created on the surface. The alloy with a lower dissolution value was Ti-6Al-2Sn-4Zr-2Mo, with 121.12 dBi $(A^2 \cdot Hz^{-1})^{1/2}$. Maybe the results do not match with corrosion rates obtained in CPP, but they match with the kinetic behavior of the CPP return. This occurs because EN is a sensitive technique that measures the passive layer's behavior created. The dissolution showed in PSD in ECN corresponds to the passive layer created and the stability of this one.

The slope analysis shown in table 5 shows that only Ti CP2 presented uniform corrosion, and Ti-6Al-2Sn-4Zr-2Mo and Ti-6Al-4V showed values related to the pitting process. However, according to different research, the alloys presented changes in slope along with the frequencies, meaning a change in passivity or a decrease in pitting rate. Also, this is the passive layer's behavior related to the passive layer's breaking and regeneration. Besides, slope analysis has limitations for passive systems and is necessary to employ alternative methods.

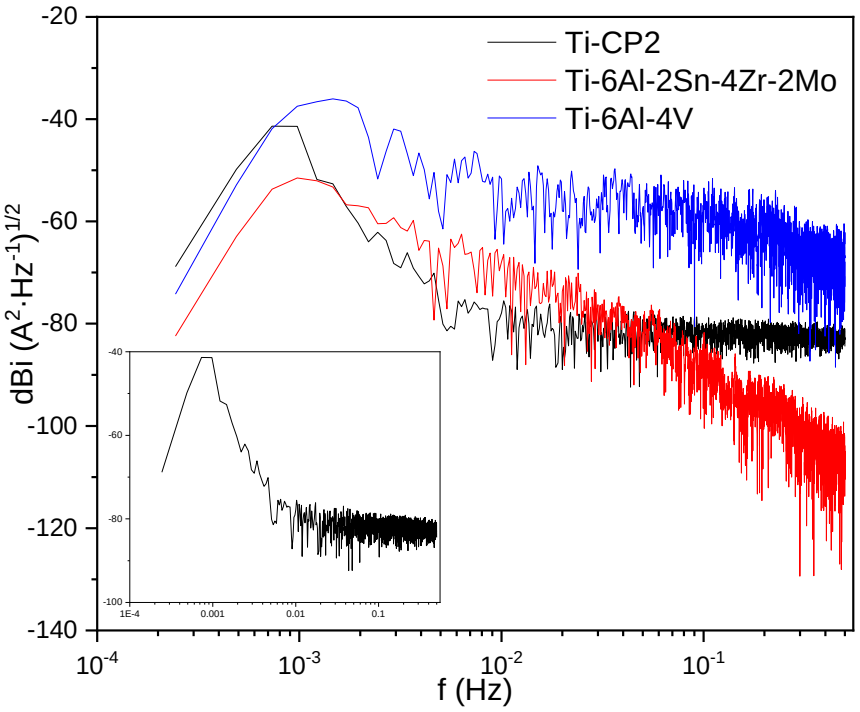

Figure 4. ECN Power Spectral Density for Titanium and its alloys exposed on Ringer´s solution.

The reaction that forms TiO_2 is slower with the presence of Cl^-, and this can be observed in PSD, where slope changes along with the frequency, meaning a breakdown and regeneration of the passive layer [46]. Also, Cl^- ions migrate to the passive layer and adhere to material and oxide as in the following chemical reaction:

$$Ti_aO_b + 2Cl^- \rightarrow Ti_aO_bCl_2 + 2e^-$$

Table 5. Parameters obtained by PSD for Titanium and its alloys exposed on Ringer´s solution.

Alloys	Ψ^0 (dBi)	B (dB [A]])
Ti CP2	–68.84	–3
Ti-6Al-2Sn-4Zr-2Mo	–82.39	–21
Ti-6Al-4V	–74.19	–9

3.2.4. Wavelets Analysis

Figure 5 shows the energy dispersion plot (EDP) for Ti CP2 and its alloys exposed to ringer solution. Ti CP2 increases energy demands in crystals D4 to D7, and this process is related to the increase of a passive layer. However, the decrease of energy in the last crystal is related to the non-diffusion of the passive layer. On the other hand, Ti 6-Al-2Sn-4Zr-2Mo and Ti-6Al-4V presented high energy accumulation in the last crystals. This mechanism is related to diffusion or uniform corrosion because it is long. Also, the energy distribution is the last crystal (special for Ti-6Al-4V); this can be related to low energy dispersion transference.

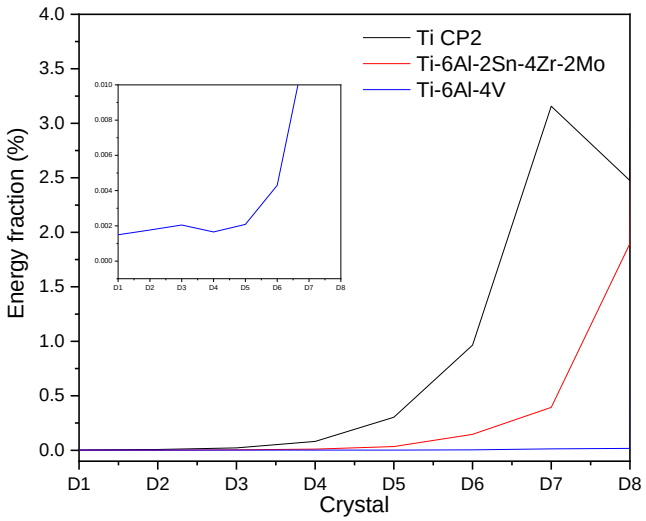

Figure 5. Energy Dispersion Plot calculated by wavelets method for Titanium and its alloys exposed on Ringer´s solution.

Authors have reported that chemical composition will play a fundamental role in the corrosion resistance of alloys [47]. Also, Cl^- attacks the surface as an interstitial element. These ions are bigger than O and Cl^- ions are difficult to create a passive layer and auspicious for the diffusion process of salts ions on the surface [48]. The changes in PSD slope (figure 4) are related to the instability the passive layer created [49].

3.3. SEM Analysis

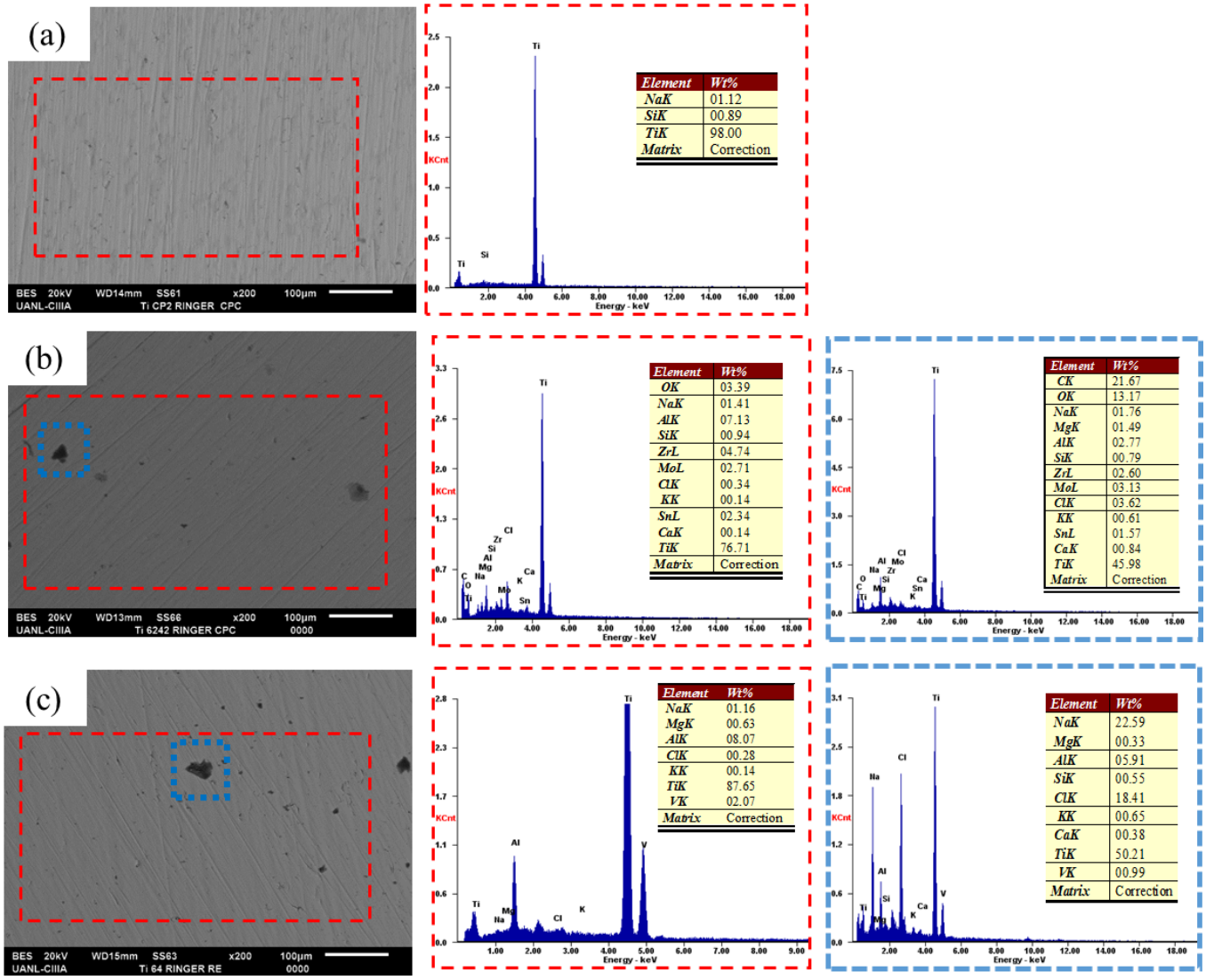

Figure 6. SEM-BES surface morphology micrographs and EDS spectrum of titanium and its alloys exposed on Ringer´s solution.

After SEM and EDS analyzed the electrochemical experiments, the corrosion products are shown in figure 6 (a, b, and c) using a backscattered electron (BSE) detector and the EDS energy spectrum for titanium and its alloys. The presence of elements such as titanium, zirconium, aluminum, molybdenum, tin, and vanadium is observed in the EDS analysis; those elements correspond to the base elements of

the alloys. All samples presented oxygen presence, meaning the development of a passive layer. However, Cl^- is shown, meaning a diffusion of elements. Cl^- is related to the low oxygen percentage because Cl ions avoid the uniform development of the passive layer.

As wavelets analysis showed, the presence of elements such as Cl, Na, Ca, O, and Mg denotes the diffusion of elements on the metal surface. Also, the presence of oxygen suggests that a passive layer was developed, but with the presence of ions of Na, Cl, and Mg difficult, the passivation process.

4. CONCLUSIONS

The results indicated that Ti-6Al-2Sn-4Zr-2Mo developed a more stable passive layer than the other alloys. This is due to elements such as Zr and Mo that help create a passive layer that is more resistant to corrosion. However, the passive layer created is unstable due to the presence of Cl^- ions that penetrate and attack as an interstitial element.

All samples presented uniform corrosion when PPC studied them. Also, the Wavelets method The diffusion process is related to a uniform process, which is corroborated by SEM-EDS analysis.

Results of material dissolution obtained from PSD (ψ^0) showed that Ti-6Al-2Sn-4Zr-2Mo presents less material dissolution. This result is related to the i_{corr} back, indicating the dissolution of the passive layer generated by the natural reactions.

The wavelets method is more reliable than the PSD slope method to determine the type of corrosion occurring in the system.

ACKNOWLEDGMENTS
The authors would like to thank the CONACYT for the support provided for developing the projects A1-S-8882, the UANL-CA-316 working group, and Universidad Autónoma de Nuevo León (UANL) for the facilities given to developing this investigation.

References

1. B. Su, B. Wang, L. Luo, L. Wang, Y. Su, Y. Xu, B. Li, T. Li, H. Huang, J. Guo, H. Fu, and Y. Zou, *Mater. Des.*, 214 (2022) 110416.
2. P. Bocchetta, L.-Y. Chen, J. D. C. Tardelli, A. C. dos Reis, F. Almeraya-Calderón, and P. Leo, *Coatings*, 11 (2021) 487.
3. J. Jaquez-Muñoz, J. C. Gaona-Tiburcio, A. Lira-Martinez, A.; P. Zambrano-Robledo, E. Maldonado-Bandala, O. Samaniego-Gamez, D. Nieves-Mendoza, J. Olguin-Coca, F. Estupiñan-Lopez, F. Almeraya-Calderon. *Metals,* 11 (2021), 1002
4. P. Fernandes Santos, M. Niinomi, H. Liu, K. Cho, M. Nakai, A. Trenggono, S. Champagne, H. Hermawan, and T. Narushima, *Mater. Des.*, 110 (2016) 414.
5. D. Q. Martins, W. R. Osório, M. E. P. Souza, R. Caram, and A. Garcia, *Electrochim. Acta*, 53 (2008) 2809.
6. B. Su, B. Wang, L. Luo, L. Wang, Y. Su, Y. Xu, F. Wang, B. Han, H. Huang, J. Guo, and H. Fu, *J. Mater. Res. Technol.*, 15 (2021) 4896.
7. L. C. Zhang and L. Y. Chen, *Adv. Eng. Mater.*, 21 (2019) 1801215.
8. H. Y. Kim, Y. Ikehara, J. I. Kim, H. Hosoda, and S. Miyazaki, *Acta Mater.*, 54 (2006) 2419.

9. B. Moretti, V. Pesce, G. Maccagnano, G. Vicenti, P. Lovreglio, L. Soleo, and P. Apostoli, *Lancet (London, England)*, 379 (2012) 1676.
10. R. Ion, D. M. Gordin, V. Mitran, P. Osiceanu, S. Dinescu, T. Gloriant, and A. Cimpean, *Mater. Sci. Eng. C*, 35 (2014) 411.
11. M. Chen, L. Yang, L. Zhang, Y. Han, Z. Lu, G. Qin, and E. Zhang, *Mater. Sci. Eng. C*, 75 (2017) 906.
12. Z. Liu, X. Liu, U. Donatus, G. E. Thompson, and P. Skeldon, *Int. J. Electrochem. Sci*, 9 (2014) 3558.
13. R. Corral-Higuera, S. Arredondo-Rea, M.A. Neri-Flores, J.M.Gómez-Soberón, J.L.Almaral-Sánchez, J. Castorena-González, F. Almeraya-Calderón, F. Int. J. Electrochem. Sci. 2011, 6, 958–970.
14. D. F. Ferreira, S. M. A. Almeida, R. B. Soares, L. Juliani, A. Q. Bracarense, V. D. F. C. Lins, and R. M. R. Junqueira, *J. Mater. Res. Technol.*, 8 (2019) 1593.
15. S. Noumbissi, A. Scarano, and S. Gupta, *Mater.,* 12 (2019) 368.
16. S. Attabi, M. Mokhtari, Y. Taibi, I. Abdel-Rahman, B. Hafez, and H. Elmsellem, *J. Bio- Tribo-Corrosion 2018 51*, 5 (2018) 1.
17. D. H. Xia, S. Z. Song, and Y. Behnamian, *Corr. Eng. Sci, and Tech.*, 51 (2016) 527.
18. C. Liu, A. Leyland, Q. Bi, and A. Matthews, *Surf. Coatings Technol.*, 141 (2001) 164.
19. R. Corral, H. S. Arredondo, R.M.A. Neri, F.J.M. Gómez, S.F. Almeraya, C.J. Castorena, G.J.L. Almaral. *Int. J. Electrochem. Sci*., 6 (2011) 613.
20. N. T. C. Oliveira and A. C. Guastaldi, *Acta Biomater.*, 5 (2009) 399.
21. X. Q. Du, Q. S. Yang, Y. Chen, Y. Yang, and Z. Zhang, *Trans. Nonferrous Met. Soc. China*, 24 (2014) 570.
22. S. Esmailzadeh, M. Aliofkhazraei, and H. Sarlak, *Prot. Met. Phys. Chem. Surfaces.*, 54 (2018) 976.
23. F. Estupiñán-López, F. Almeraya-Calderón, G.R.Bautista Margulis, M.A. Baltazar Zamora, A. Martínez-Villafañe, J. Uruchurtu, C. Gaona-Tiburcio, *Int. J. Electrochem. Sci*., 6 (2011) 1785.
24. ASTM E3-95. Standard Practice for Preparation of Metallographic Specimens; ASTM International: West Conshohocken, PA, USA, (1995).
25. ASTM E407-07. Standard Practice for Microetching Metals and Alloys; ASTM International: West Conshohocken, PA, USA, (2011).
26. ASTM G5-11, Standard reference test method for making potentiostatic and potentiodynamic anodic polarization measurements, West Conshohocken, PA. USA. (2011).
27. ASTM G5-11, Standard reference test method for making potentiostatic and potentiodynamic anodic polarization measurements, West Conshohocken, PA. USA. (2011).
28. J. Tafel, *Zeitschrift Für Phys. Chemie*, 50U (1905) 641.
29. M. Lara-Banda, C. Gaona-Tiburcio, P. Zambrano-Robledo, M. Delgado-E. J. Cabral-Miramontes, D. Nieves-Mendoza, E. Maldonado-Bandala, F. Estupiñan-López, J. Chacón-Nava, F. Almeraya-Calderón, F. Materials 2020, 13, 2836,
30. C. Wagner and W. Traud, *Zeitschrift Für Elektrochemie Und Angew. Phys. Chemie*, 44 (1938) 391.
31. J. A. V. Butler, *Trans. Faraday Soc.*, 19 (1924) 729.
32. T. Erdey-Grúz and M. Volmer, *Zeitschrift Für Phys. Chemie*, 150A (1930) 203.
33. ASTM G199-09. Standard Guide for Electrochemical Noise Measurement; ASTM International: West Conshohocken, PA, USA, (2009).
34. J. M. Jáquez-Muñoz, C. Gaona-Tiburcio, J. Cabral-Miramontes, D. Nieves-Mendoza, E. Maldonado-Bandala, J. Olguín-Coca, L. D. López-Léon, J. P. F. De Los Rios, and F. Almeraya-Calderón, *Metals. 2021, 11,* (2021) 105.
35. D.L. Dawson, STP 1277; Kearns, J.R., Scully, J.R., Roberge, P.R., Reirchert, D.L., Dawson, L., Eds.; ASTM International, Materials Park: USA, 1996; pp. 3–39.
36. M. Nabhani, R. Shoja Razavi, and M. Barekat, *Eng. Fail. Anal.*, 97 (2019) 234.
37. U. Bertocci and F. Huet, *Corrosion*, 51 (1995) 131.
38. C. C. Lee and F. Mansfeld, *Corros. Sci.*, 40 (1998) 959.

39. A. Legat and V. Doleček, *Corrosion.*, 51 (1995) 295.
40. A. M. Homborg, C. F. Leon Morales, T. Tinga, J. H. W. De Wit, and J. M. C. Mol, *Electrochim. Acta*, 136 (2014) 223.
41. J.A Sedriks, S.A. Green, L.D. Novak, *Corrosion*, 28 (1972) 137.
42. K. H. W. Seah, R. Thampuran, S. H. Teoh, *Corros. Sci.*, 40 (1998) 547.
43. C. Kuphasuk, Y. Oshida, C. J. Andres, S. T. Hovijitra, M. T. Barco, and D. T. Brown, *J. Prosthet. Dent.*, 85 (2001) 195.
44. C. Vasilescu, S. I. Drob, E. I. Neacsu, and J. C. Mirza Rosca, *Corros. Sci.*, 65 (2012) 431.
45. J. Dias Corpa Tardelli, C. Bolfarini, and A. Cândido dos Reis, *J. Trace Elem. Med. Biol.*, 62 (2020) 126618.
46. G. Adamek, K. Pałka, and J. Jakubowicz, *Solid State Phenom.*, 227 (2015) 519.
47. P. W. Doll, M. Wolf, M. Weichert, R. Ahrens, B. Spindler, and A. E. Guber, *Curr. Dir. Biomed. Eng.*, 4 (2018) 641.
48. X. Chen, Q. Fu, Y. Jin, M. Li, R. Yang, X. Cui, and M. Gong, *Mater. Sci. Eng. C*, 70 (2017) 1071.
49. A. Contreras, M. Salazar, A. Carmona, and R. Galván-Martínez, *Mater. Res.*, 20 (2017) 1201.